Bifurcated Polarization Rotation in Bismuth-Based Piezoelectrics

Dean S. Keeble, Emma R. Barney, David A. Keen, Matthew G. Tucker, Jens Kreisel, and Pam A. Thomas*

ABO_3 perovskite-type solid solutions display a large variety of structural and physical properties, which can be tuned by chemical composition or external parameters such as temperature, pressure, strain, electric, or magnetic fields. Some solid solutions show remarkably enhanced physical properties including colossal magnetoresistance or giant piezoelectricity. It has been recognized that structural distortions, competing on the local level, are key to understanding and tuning these remarkable properties, yet, it remains a challenge to experimentally observe such local structural details. Here, from neutron pair-distribution analysis, a temperature-dependent 3D atomic-level model of the lead-free piezoelectric perovskite $Na_{0.5}Bi_{0.5}TiO_3$ (NBT) is reported. The statistical analysis of this model shows how local distortions compete, how this competition develops with temperature, and, in particular, how different polar displacements of Bi^{3+} cations coexist as a bifurcated polarization, highlighting the interest of Bi-based materials in the search for new lead-free piezoelectrics.

1. Introduction

Piezoelectrics, i.e., materials with coupled electric and strain fields, find industrial usage in a wide range of applications.[1,2] Most commercial piezoelectric devices use lead-based solid solutions such as $PbZr_{1-x}Ti_xO_3$ (PZT) or $Pb(Mg_{1/3}Nb_{2/3})_{1-x}Ti_xO_3$ (PMN-PT) that undergo a compositionally driven phase transition from rhombohedral (R) to tetragonal (T) symmetry, via a much discussed transitional region called the morphotropic phase boundary (MPB).[1] It has been recently shown[3] that the average structure of the MPB in PZT and similar materials can be described in monoclinic symmetry, which allows for a continuous polarization rotation from R to T through a monoclinic plane, leading to an electrically soft material. The phase transition via such a polarization rotation has generally been considered to be at the origin of the high piezoelectric response,[4] although other nanodomain-based mechanisms are proposed.[5]

A growing concern regarding the toxicity in lead-containing devices, and thus their environmental impact, has triggered a considerable interest in lead-free piezoelectrics.[6,7] Because of its electronic similarity with Pb^{2+}, the "lone-pair" cation Bi^{3+} appears as a natural replacement candidate and, in some Bi^{3+}-based perovskites, produces a similarly large ferroelectric polarization. Bismuth perovskites are often difficult to stabilize at ambient pressure because of the small size of the Bi^{3+} ion, for instance both $BiCrO_3$ and $BiMnO_3$ require high-pressure synthesis, and this difficulty has hampered wider investigations and understanding. Thus the majority of studies have focussed on only two stable materials: the multiferroic bismuth ferrite $BiFeO_3$ with a reported strain-driven MPB in thin films,[8] and $Na_{0.5}Bi_{0.5}TiO_3$ (NBT), which presents a high piezoelectric response[9] when doped with Ba^{2+}. Beyond the simple idea of replacing Pb^{2+} with a similar cation, an attractive attribute of bismuth-containing perovskites is the observed disinclination of Bi^{3+} to produce a particular distortion, suggesting a particularly adaptive chemical bond.[10] Whereas in the absence of any external stimuli, Pb^{2+} will undergo a tetragonal distortion (as in $PbTiO_3$ or $PbVO_3$), there are examples of Bi^{3+} being accommodated in rhombohedral symmetry ($BiFeO_3$),[11] triclinic and orthorhombic symmetry ($BiMnO_3$),[12] or monoclinic symmetry ($BiCrO_3$)[13] at ambient conditions. This chemical richness is underlined by reports of an unusually large number of competing structures of similar energy in strained $BiFeO_3$ thin films[14] or $BiFeO_3$ crystals at high pressure.[15]

Within this context, we have chosen to investigate in detail $Na_{0.5}Bi_{0.5}TiO_3$ (NBT), a starting material for numerous NBT-based lead-free piezoelectrics,[7] some of which surpass even the properties of PZT.[16] On the average scale, NBT undergoes a thermally driven phase transition sequence from a room

Dr. D. S. Keeble, Prof. P. A. Thomas
Department of Physics
University of Warwick
Gibbet Hill Road, Coventry, CV4 7AL, UK
E-mail: d.s.keeble@warwick.ac.uk
Dr. E. R. Barney
Faculty of Engineering
University of Nottingham
Nottingham NG7 2RD, UK
Prof. D. A. Keen, Dr. M. G. Tucker
ISIS Facility, Rutherford Appleton Laboratory
Harwell Oxford, Didcot, Oxfordshire, OX11 0QX, UK
Prof. J. Kreisel
Science and Analysis of Materials
CRP Gabriel Lippmann, 41, Rue du Brill
4422 Bevalux Luxembourg
and Laboratoire des Matériaux et du Génie Physique
Grenoble INP, CNRS, Minatec, 38016 Grenoble, France

DOI: 10.1002/adfm.201201564

temperature rhombohedral structure to a peculiar tetragonal symmetry[17] at 528 K, and further at 800 K to a cubic structure.[18] More recently some evidence for long-range non-rhombohedral distortions has been discussed.[19,20] Importantly, the local structure of NBT shows significant nano-scale deviations from the average structure, as for instance observed by diffuse scattering,[21] extended X-ray absorption fine structure (EXAFS)[22] or transmission electron microscopy.[23,24] However, to date, there is no understanding of the local competing interactions: in order to explain the remarkable piezoelectric properties, we need to understand how these interactions determine the average structure, and influence phase sequences. Here, we aim to establish a 3D atomic-level model of NBT in order to provide a better understanding of its unusual structural and physical properties. Given the importance of bismuth in a number of functional oxides, including the model multiferroic $BiFeO_3$,[25] we specifically focus on the Bi^{3+} environment in terms of the size and direction of polar displacements on a local level.

For our investigation into the complex atomic arrangement we have conducted a neutron total scattering experiment. Neutron scattering presents the advantage over X-ray scattering or TEM that the light oxygen atoms contribute significantly to the overall scattering intensities, which is important given that oxygens form the perovskite connectivity: the octahedral network provides the reference frame for the calculation of local cation displacements. The strength of total scattering lies in the fact that it includes both Bragg scattering, which provides information on the average structure, and diffuse scattering, which is characteristic of short- and medium-range order.[26] The common method used to analyse total scattering data is by studying its Fourier transform, yielding the pair distribution function (PDF), which expresses in real space the probability of finding two atoms separated by a distance *r*. In NBT such a total PDF is the weighted sum of ten constituent atom-specific "partial" PDFs, which we have extracted via structural modelling using the Reverse Monte-Carlo (RMC) algorithm RMCProfile.[27] Generally speaking, the PDF technique has been shown to be a powerful probe of average local structural details,[26,28] able also to guide and countercheck ab initio calculations.[29] In the present case, we built as a starting model a >7000 atom supercell, based on the Rietveld-refined average structure at each temperature, which has then undergone a large number of RMC iterations against the experimental PDF data (see Supporting Information).

2. Results

In a first step, we compare in **Figure 1**a the experimental neutron PDFs obtained for NBT at four different temperatures of 10, 298, 473 and 766 K, to PDFs simulated from two reported average structures of rhombohedral[18] and monoclinic[20] symmetry. The overall form of the PDF is at first sight similar for the simulated and experimental PDFs, particularly for distances longer than 3.5 Å and for the negative feature around 2 Å, which arises from the Ti–O bond in the TiO_6 octahedra. However, there is significant disagreement in the region from 2 to 3.5 Å, where the average-structure simulated PDFs give one broad positive peak while the experimental PDFs show a fine structure of additional features at 2.2 Å and 3.2 Å, together with a sharpened main peak at 2.77 Å. Considering the atomic arrangement in a perovskite structure, we conclude that the extra features are due to either Bi-O or the Na-O correlations. Inspection of the Bi-O and Na-O partial PDFs in Figure 1b, obtained from the atomic model, suggests that the Bi-O correlations account for the low-*r* shoulder at 2.2 Å, in agreement with previous Bi^{3+} EXAFS studies,[22] while the 3.2 Å shoulder contains contributions from both Na-O and Bi-O correlations. The comparison of the experimental PDFs with the average structure PDFs thus confirms that the local structure of NBT is significantly different from the average structure and suggests that this difference mostly relates to the *A*-site of the ABO_3 perovskite structure.

In order to identify and analyse the element-specific local structural details we turn in more detail to the structural models from the RMC fitting. The so-obtained models were statistically analysed in order to identify the direction (symmetry) and size of atomic displacements of each Na, Bi and Ti-cation from the centroid of the surrounding oxygen polyhedral cage.

We first present in **Figure 2** the outcome of this statistical analysis for the direction of displacement by plotting them in the form of a stereographic projection. This is a convenient way to distinguish displacements along a rhombohedral (R hereafter, $\langle 111\rangle_{\text{pseudo cubic}}$), tetragonal (T, $\langle 001\rangle_{pc}$), orthorhombic (O, $\langle 110\rangle_{pc}$) direction, or within a monoclinic (M, $\{110\}_{pc}$) plane. Our analysis shows that the Ti-cations are, even in the high-temperature phase, displaced predominantly along rhombohedral $\langle 111\rangle_{pc}$ directions (see Figure S1, Supporting Information), which is reminiscent of $BaTiO_3$ (ref. [30]). The situation

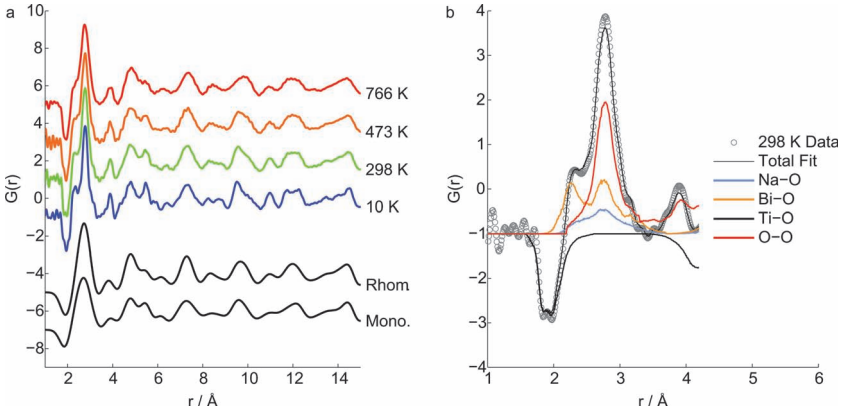

Figure 1. Pair distribution function (PDF) data from $Na_{0.5}Bi_{0.5}TiO_3$ (NBT) and comparison to average structure. a) The PDF data at 10 K (blue); 298 K (green); 473 K (orange) 766 K (red); and two simulated G(r) from the room-temperature Rietveld-refined structures in rhombohedral[18] and monoclinic[20] symmetry, (black), demonstrating the absence of the peaks at 2.2 Å and 3.2 Å in the average Rietveld structures. b) Short *r* partial g(r) for Na-O (blue), Bi-O (orange), Ti-O (black) and O-O (red) correlations, as calculated using RMC modelling of the data, along with the observed total G(r) and fit from the modelling, demonstrating the disparity between the local environment of sodium and bismuth.

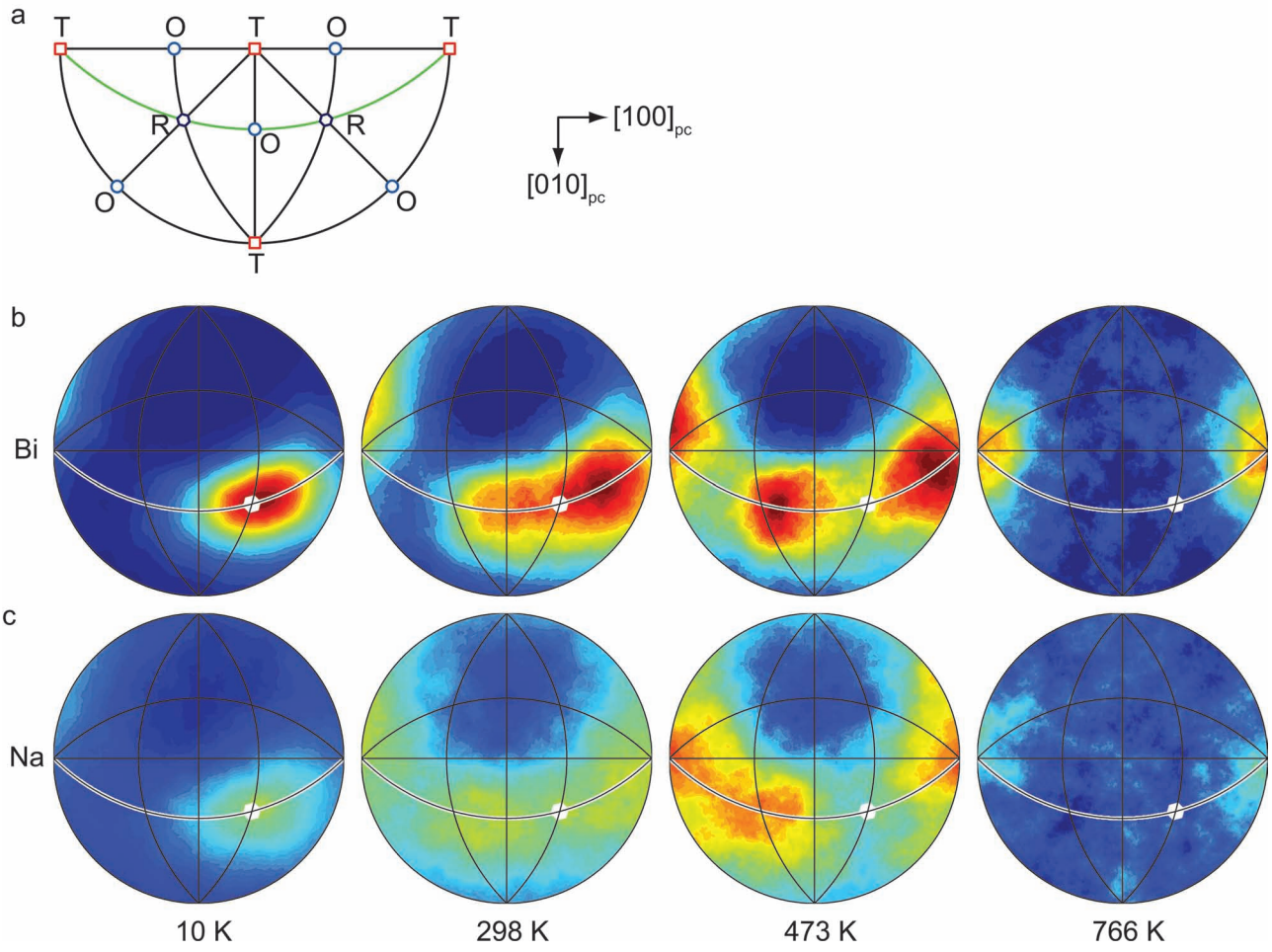

Figure 2. A-site displacement directions. a) Schematic of the key symmetry-defining displacement directions in pseudo-cubic perovskites: tetragonal symmetry is defined by displacements along $\langle 100 \rangle_{pc}$-type directions (T, red squares), orthorhombic by $\langle 110 \rangle_{pc}$ directions (O, blue circles), rhombohedral by $\langle 111 \rangle_{pc}$ (R, black hexagon); monoclinic by $\{110\}_{pc}$ planes (M, one of which is highlighted in green), and triclinic elsewhere. b,c) Stereographic projections of bismuth (b) and sodium (c) displacements from the centroid of the individual coordination polyhedra. The intensity of the contours is proportional to the number of individual displacements that lie close to that direction. The rhombohedral polar direction is highlighted as a white hexagon in each panel, and the relevant monoclinic plane is highlighted as the white solid line.

is fundamentally different for the displacements of the Bi^{3+} and Na^{+} atoms, which significantly change over the four investigated temperatures: i) $T = 10$ K: at low temperature, both the sodium and the bismuth displace predominantly along the $[111]_{pc}$ direction, although with a small distribution of directions in the monoclinic plane (Figure 2b,c). Since the Ti-cations displace along the same rhombohedral direction, there is a long-range concerted distortion that invokes the rhombohedral structure, as assigned by previous authors.[31] ii) $T = 298$ K: when the temperature is increased the intensities of both the bismuth and the sodium smear out along the monoclinic plane. The bismuth displacements are characterized by two semi-distinct points, one directed in the monoclinic plane (hereafter denoted $Bi^{(I)}$) and the other one approaching the orthorhombic $[011]_{pc}$ direction (denoted $Bi^{(II)}$). $Bi^{(I)}$, the more populated displacement direction, points towards $[1\ 0.41\ 0.41]_{pc}$, which, interestingly, is closely parallel to the displacement direction calculated from the recently proposed room-temperature monoclinic structure.[20] By contrast, the sodium displace within the monoclinic plane with no visible preference for a specific direction. iii) $T = 473$ K: the splitting of the two predominant bismuth positions $Bi^{(I)}$ and $Bi^{(II)}$ becomes more pronounced with increasing temperature, showing now two well-separated displacements of equivalent weight inside the monoclinic plane. We note that these two monoclinic displacements approach the R- and T-points: directions which are already predominantly adopted by the Na^{+} cations. iv) $T = 766$ K: now, the Bi^{3+} displacements point along a single T-direction, with little smearing. The sodium displacement directions are more disordered than the corresponding bismuths, as emphasised by the less intense features in the stereographic projection, most likely because of the small size of their displacements.

Now armed with this local view of the structure, we recall that the average structure at 10, 298 and 473 K is, to a good approximation, rhombohedral,[31] while the 766 K average structure is tetragonal.[18] To investigate the average structure of our disordered model, we calculate the mean polar bismuth displacement, which at 10, 298 and 473 K is inclined from the

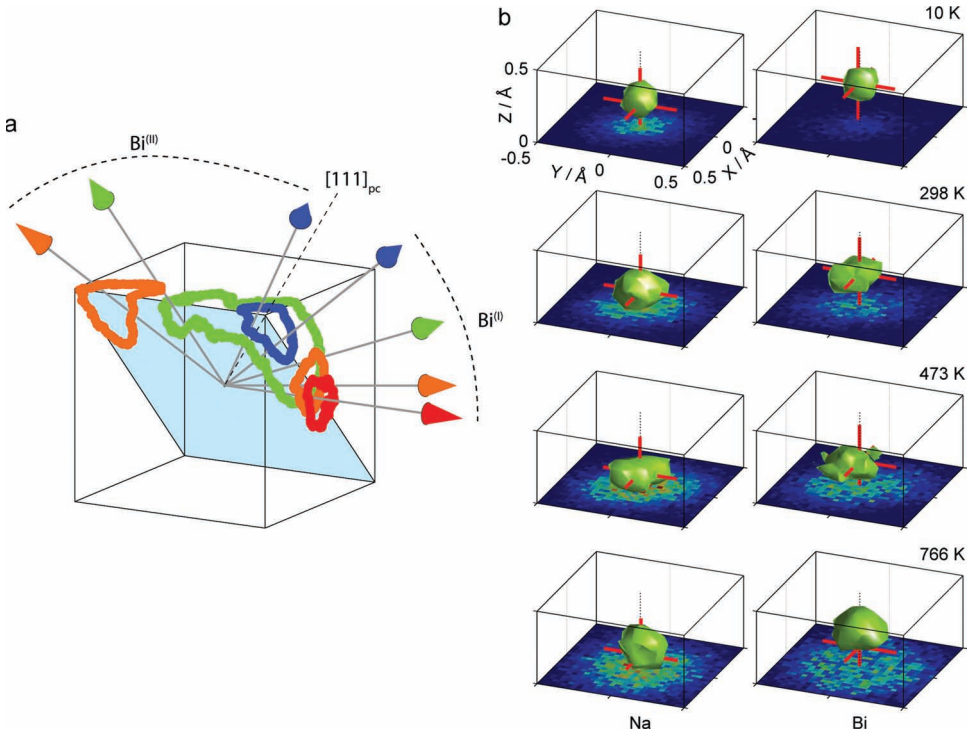

Figure 3. Temperature evolution of the A-site local environment. a) Schematic of the two polarization rotations within the perovskite structure seen as a function of temperature, from 10 K (blue) to 766 K (red). The contours are taken from the stereograms in Figure 2, projected onto the surface of a prototypic cube. The arrows denote predominant displacement directions. b) Density plots of displacement vectors for Na^+ and Bi^{3+} at various temperatures, with isosurfaces showing contours at 75% of normalised density. The panels are rotated such that the Rietveld-refined polar directions are all along +z, therefore the horizontal slice is normal to the polar direction (i.e., normal to $[001]_{pc}$ at 766 K; normal to $[111]_{pc}$ at lower temperatures) and crosses the polar direction at $z = 0$. The mean displacement is bisected in these images by the red, 0.5 Å long crosshairs.

[111] direction by less than 2.5° (see Table S1, Supporting Information). This observation confirms that the average structure can indeed be described by a rhombohedral model and that the local structure observed here is entirely consistent with the reported average structure. Similarly for the high-temperature model, the observed average structure is tetragonal, i.e. the four Ti rhombohedral displacement directions (see Figure S1, Supporting Information) lead to an average tetragonal distortion, opposed in direction to the overall polar direction, as defined by the strong bismuth distortions.

Further to the direction of displacement, the analysis of the RMC modelling also allows identification of the real-space distributions of the size of displacements. **Figure 3**a shows a plot of the density of displacements, where the middle cross indicates the position of the mean displacement. The shapes of these surfaces confirm that as the temperature is increased the distributions of the displacements become more anisotropic, appearing more elongated away from the polar axis than along it. The comparison of the two *A*-site species shows that Bi^{3+} is significantly more displaced along the polar direction than Na^+ (Bi: 0.131 to 0.285 Å, Na: 0.080 to 0.142 Å) at all investigated temperatures. Whilst this is in agreement with common crystal-chemistry knowledge for the chemically very different A-site cations, its direct experimental observation in a scattering experiment is, we believe, a first, particularly given that the starting model contained sodium and bismuth with identical local structures.

Altogether, the analysis of the direction and size of cation displacements shows that the local structure of NBT is characterised by competing structural distortions between both the varying symmetries on the *A*-site and the rhombohedral symmetry of the Ti-cations; and also between distinct displacements on the *A*-site (Na vs. Bi and $Bi^{(I)}$ vs. $Bi^{(II)}$).

The most extraordinary feature of our analysis is the coexistence of two dominating directions of bismuth cation displacement, particularly at higher temperatures within the rhombohedral phase. The stereographic projections in Figure 2 show that both directions are confined to a monoclinic plane, but it is interesting to observe that the two displacements actually counter-rotate through this plane as the temperature is increased. As a consequence, neither a polarization-rotation nor a co-existence model can entirely explain the phase sequence, but rather two co-existing polarization rotations are necessary: we refer to this as bifurcated polarization rotation. The rotation of polarization with temperature is illustrated in Figure 3b as extracted contours from the stereographic projections. It is important to realize that the two rotation-paths involve different phase sequences for which we have snapshots at four temperatures. Figure 3a illustrates that the rotation of $Bi^{(I)}$ starts close to *R* and then rotates at 298 and 473 K through a single monoclinic segment towards *T*. This monoclinic segment has been earlier termed[32] M_A and allows for a continuous second order-type rotation with the temperature phase sequence $R \rightarrow M_A \rightarrow T$,

analogous to the morphotropic phase boundary sequence in highly piezoelectric lead-based perovskites. By contrast, $Bi^{(II)}$ starts close to *R* in a different monoclinic segment denoted M_B,[32] rotates towards O, then into an equivalent M_B segment before finally adopting a tetragonal T displacement, leading to a $R \rightarrow M_B \rightarrow O \rightarrow M_B$ (→) T phase sequence. Although the limited number of available snapshots does not allow continuous following of all details of the $Bi^{(II)}$ rotation (namely the transition $M_B \rightarrow T$), it is observed that $Bi^{(I)}$ and $Bi^{(II)}$ undergo different transition sequences, leading to complex nano- or microstructures at 298 and 473 K. The observation of a complex birefringence[33] in NBT, including the recent observation of an optical isotropization, pinpointed as occuring just before the entrance into the tetragonal phase,[34] support the suggestion of a locally biphasic transition such as that observed here.

3. Discussion

We believe that the coexistence of $Bi^{(I)}$ and $Bi^{(II)}$, and thus two distortions, within the same phase arises from two factors: first, both distortions are very close in energy; and second, the material inherently manifests both local random electric fields (because of the Na^+/Bi^{3+} charge difference) and random elastic fields (because of the different size and shape of BiO_{12} and NaO_{12}) (see Figure S2, Supporting Information). This situation is reminiscent of the competing and energetically similar monoclinic structures in $BiFeO_3$, the actual state of which can be driven by slight differences of strain in thin films,[8,14] and is consistent with recent observations of multiple disorder types.[24] For NBT, the obvious way to tune this local structural competition is by chemical substitution, which allows variation of both local electric and elastic fields, which in turn is expected to have a significant impact on the physical properties. With this in mind, it is now interesting to consider some of the numerous solid solutions that have been investigated in the literature. When NBT is doped by barium, a cation with a different 2+ charge and a ≈ 20% larger ionic size than sodium or bismuth, a large enhancement of piezoelectric properties is observed,[9] in contrast to the isovalent substitution in $(Na_{1-x}K_x)_{0.5}Bi_{0.5}Ti_{0.5}O_3$. Interestingly, it has been shown[16] that more complex solid solutions like $Na_{0.5}Bi_{0.5}TiO_3$-$BaTiO_3$-$K_{0.5}Na_{0.5}NbO_3$, which also modifies the charges and sizes on *B*-sites, display to date the most enhanced piezoelectric properties in NBT-based materials. This further underlines the importance of the *B*-site cation in influencing the bismuth direction of displacement, a point which is worthy of more attention.

Bifurcated directions of bismuth displacement coexist in NBT, underlining bismuth's ability to adopt different types of polarization directions in perovskites: these can then be tuned by chemical substitution to modify the local electric and elastic fields. This structural softness is an important property sought in piezoelectric materials and this observation should motivate crystal chemists to overcome the inherent synthesis difficulties in bismuth-based materials, both perovskite and other, in the search for new high-performance lead-free piezoelectrics. The PDF-based approach presented here is widely applicable to the study of other complex perovskites and has the potential to reveal either completely unknown or suspected-but-unproven structural competitions on the local level.

4. Experimental Section

Sample Fabrication: A polycrystalline sample of $Na_{0.5}Bi_{0.5}TiO_3$ was produced following the method prescribed elsewhere,[17] after which the powder was reground and sieved to a particle size of <10 μm.

Neutron Total-Scattering Data Collection: Total scattering patterns were collected at a range of temperatures using the neutron time-of-flight diffractometer GEM[35] at the ISIS pulsed neutron spallation source, Rutherford Appleton Laboratory, Oxfordshire, UK. High quality data were obtained to a Q of ≈40 $Å^{-1}$, and were reduced and corrected for attenuation, inelasticity effects, multiple scattering and background using standard Gudrun and ATLAS[36] software. The corrected total scattering structure factors, $F(Q)$, were then Fourier transformed and normalised to give the total radial distribution function, $G(r)$.[37]

Reverse Monte Carlo Refinement: Reverse Monte Carlo (RMC) modelling was implemented using the package RMCProfile.[27,38] Initial iterations of the algorithm were performed whilst fitting just the $G(r)$ and $F(Q)$ data (i.e., with no Bragg profile data)[39] with bond valence sum constraints[40] and realistic distance window constraints, to ensure the general perovskite connectivity was maintained. Once this refinement had converged, final models were produced by additionally fitting the Bragg profile data, with an increased weighting of the $F(Q)$ data. In order to improve the statistics of the results, each temperature's data were modelled 120 times.

Supporting Information

Supporting Information is available from the Wiley Online Library or from the author.

Acknowledgements

The authors thank S. Gorfman for assistance with the data analysis, D. Walker for his assistance with the data collection, and STFC for provision of neutron beam time. Computing resources were provided by STFC's e-Science facility. D.S.K. thanks the Science City Research Alliance and the HEFCE Strategic Development Fund for financial support. J.K. acknowledges financial support during his sabbatical stay at Warwick University from the Institute of Advanced Study (IAS) Warwick and from the Région Rhône-Alpes (CMIRA grant).

Received: June 11, 2012
Revised: July 30, 2012
Published online: August 22, 2012

[1] B. Jaffe, W. R. Cook, H. Jaffe, *Piezoelectric Ceramics*, Academic Press, London **1971**.
[2] G. H. Haertling, *J. Am. Ceram. Soc.* **1999**, *82*, 797.
[3] B. Noheda, D. E. Cox, G. Shirane, J. A. Gonzalo, L. E. Cross, S. E. Park, *Appl. Phys. Lett.* **1999**, *74*, 2059.
[4] a) R. Guo, L. E. Cross, S. E. Park, B. Noheda, D. E. Cox, G. Shirane, *Phys. Rev. Lett.* **2000**, *84*, 5423; b) H. Fu, R. E. Cohen, *Nature* **2000**, *403*, 281.
[5] a) Y. M. Jin, Y. U. Wang, A. G. Khachaturyan, J. F. Li, D. Viehland, *J. Appl. Phys.* **2003**, *94*, 3629; b) R. Theissmann, L. A. Schmitt, J. Kling, R. Schierholz, K. A. Schonau, H. Fuess, M. Knapp, H. Kungl, M. J. Hoffmann, *J. Appl. Phys.* **2007**, *102*, 024111.
[6] a) Y. Saito, H. Takao, T. Tani, K. Nonoyama, K. Takatori, T. Homma, T. Nagaya, M. Nakamura, *Nature* **2004**, *432*, 84; b) M. D. Maede, D. Damjanovic, N. Setter, *J. Electroceram.* **2004**, *13*, 395.
[7] J. Rodel, W. Jo, K. T. P. Seifert, E. M. Anton, T. Granzow, D. Damjanovic, *J. Am. Ceram. Soc.* **2009**, *92*, 1153.
[8] R. J. Zeches, M. D. Rossell, J. X. Zhang, A. J. Hatt, Q. He, C. H. Yang, A. Kumar, C. H. Wang, A. Melville, C. Adamo, G. Sheng,

Y. H. Chu, J. F. Ihlefeld, R. Erni, C. Ederer, V. Gopalan, L. Q. Chen, D. G. Schlom, N. A. Spaldin, L. W. Martin, R. Ramesh, *Science* **2009**, *326*, 977.
[9] Y.-M. Chiang, G. W. Farrey, A. N. Soukhojak, *Appl. Phys. Lett.* **1998**, *73*, 3683.
[10] D. Schütz, M. Deluca, W. Krauss, A. Feteira, T. Jackson, K. Reichmann, *Adv. Funct. Mater.* **2012**, *22*, 2285.
[11] J. M. Moreau, C. Michel, R. Gerson, W. J. James, *J. Phys. Chem. Solids* **1971**, *32*, 1315.
[12] I. O. Troyanchuk, N. V. Samsonenko, E. F. Shapovalova, I. M. Kolesova, H. Shymczak, *J. Phys. Condens. Matter* **1996**, *8*, 11205.
[13] T. Atou, H. Chiba, K. Ohoyama, Y. Yamaguchi, Y. Syono, *J. Solid State Chem.* **1999**, *145*, 639.
[14] O. Diéguez, O. E. González-Vázquez, J. C. Wojdeł, J. Íñiguez, *Phys. Rev. B* **2011**, *83*, 094105.
[15] M. Guennou, P. Bouvier, G. S. Chen, R. Haumont, G. Garbarino, J. Kreisel, *Phys. Rev. B* **2011**, *84*, 174107.
[16] a) S.-T. Zhang, A. B. Kounga, E. Aulbach, T. Granzow, W. Jo, H.-J. Kleebe, J. Rodel, *J. Appl. Phys.* **2008**, *103*, 034107; b) S.-T. Zhang, A. B. Kounga, E. Aulbach, W. Jo, T. Granzow, H. Ehrenberg, J. Rodel, *J. Appl. Phys.* **2008**, *103*, 034108.
[17] G. O. Jones, P. A. Thomas, *Acta Crystallogr. B* **2000**, *56*, 426.
[18] G. O. Jones, P. A. Thomas, *Acta Crystallogr. B* **2002**, *58*, 168.
[19] S. Gorfman, P. A. Thomas, *J. Appl. Crystallogr.* **2010**, *43*, 1409.
[20] E. Aksel, J. S. Forrester, J. L. Jones, P. A. Thomas, K. Page, M. R. Suchomel, *Appl. Phys. Lett.* **2011**, *98*.
[21] J. Kreisel, P. Bouvier, B. Dkhil, P. A. Thomas, A. M. Glazer, T. R. Welberry, B. Chaabane, M. Mezouar, *Phys. Rev. B* **2003**, *68*, 014113.
[22] V. A. Shuvaeva, D. Zekria, A. M. Glazer, Q. Jiang, S. M. Weber, P. Bhattacharya, P. A. Thomas, *Phys. Rev. B* **2004**, *71*, 174114.
[23] V. Dorcet, G. Trolliard, *Acta Mater.* **2008**, *56*, 1753.
[24] I. Levin, I. M. Reaney, *Adv. Funct. Mater.* DOI:10.1002/adfm.201200282.
[25] G. Catalan, J. F. Scott, *Adv. Mater.* **2009**, *21*, 2463.
[26] T. Egami, S. J. L. Billinge, *Underneath the Bragg peaks: structural analysis of complex materials*, Pergamon, Amsterdam **2003**.
[27] M. G. Tucker, D. A. Keen, M. T. Dove, A. L. Goodwin, Q. Hui, *J. Phys.: Condens. Matter* **2007**, *19*, 335218.
[28] S. Y. Chong, R. J. Szczecinski, C. A. Bridges, M. G. Tucker, J. B. Claridge, M. J. Rosseinsky, *J. Am. Chem. Soc.* **2012**, *134*, 5836.
[29] a) I. Grinberg, V. L. Cooper, M. Rappe, *Nature* **2002**, *419*, 909; b) C. Laulhé, A. Pasturel, F. Hippert, J. Kreisel, *Phys. Rev. B* **2010**, *82*, 132102.
[30] R. Comès, M. Lambert, A. Guinier, *Solid State Commun.* **1970**, *6*, 715.
[31] G. A. Smolenskii, V. A. Isupov, A. I. Agranovskaya, N. N. Krainik, *Sov. Phys. Solid State* **1960**, *2*, 4.
[32] D. Vanderbilt, M. H. Cohen, *Phys. Rev. B* **2001**, *63*, 094108.
[33] M. Geday, J. Kreisel, K. Roleder, A. M. Glazer, *J. Appl. Crystallogr.* **2000**, *33*, 909.
[34] S. Gorfman, A. M. Glazer, Y. Noguchi, M. Miyayama, H. Luo, P. A. Thomas, *J. Appl. Crystallogr.* **2012**, *45*, 444.
[35] A. C. Hannon, *Nucl. Instrum. Methods A* **2005**, *551*, 88.
[36] A. C. Hannon, W. S. Howells, A. K. Soper, *IOP Conf. Ser.* **1990**, *107*, 193.
[37] D. A. Keen, *J. Appl. Crystallogr.* **2001**, *34*, 172.
[38] M. T. Dove, M. G. Tucker, D. A. Keen, *Eur. J. Mineral.* **2002**, *14*, 331.
[39] Since the calculation of the fit of $F(Q)$ uses a different algorithm to that of the Bragg profile data, RMCProfile can fit both data sets concurrently.
[40] S. T. Norberg, M. G. Tucker, S. Hull, *J. Appl. Crystallogr.* **2009**, *42*, 179.